

Molecular profiling of reticular gigantocellularis neurons indicates that eNOS modulates environmentally dependent levels of arousal

Inna Tabansky^{a,b,1}, Yupu Liang^c, Maya Frankfurt^{a,d,e,f}, Martin A. Daniels^a, Matthew Harrigan^c, Sarah Stern^{g,h}, Teresa A. Milnerⁱ, Rebecca Leshan^a, Rrezarta Rama^a, Tabea Moll^a, Jeffrey M. Friedman^{g,h}, Joel N. H. Stern^{a,b,d,e,f,j,1,2}, and Donald W. Pfaff^{a,1,2}

^aLaboratory of Neurobiology and Behavior, The Rockefeller University, New York, NY 10065; ^bFeinstein Institute for Medical Research, Manhasset, New York, NY 11030; ^cCenter for Clinical and Translational Science, The Rockefeller University, New York, NY 10065; ^dDepartment of Neurology, Zucker School of Medicine at Hofstra/Northwell, Hempstead, NY 11549; ^eDepartment of Surgery, Zucker School of Medicine at Hofstra/Northwell, Hempstead, NY 11549; ^fDepartment of Science Education, Zucker School of Medicine at Hofstra/Northwell, Hempstead, NY 11549; ^gLaboratory of Molecular Genetics, The Rockefeller University, New York, NY 10065; ^hHoward Hughes Medical Institute, The Rockefeller University, New York, NY 10065; ⁱBrain and Mind Research Institute, Weill Cornell Medical College, New York, NY 10065; and ^jDepartment of Neurology, Lenox Hill Hospital, Northwell Health, New York, NY 10075

Contributed by Donald W. Pfaff, June 6, 2018 (sent for review April 13, 2018; reviewed by Marie-Françoise Chesselet and Edgar Garcia-Rill)

Neurons of the medullary reticular nucleus gigantocellularis (NGC) and their targets have recently been a focus of research on mechanisms supporting generalized CNS arousal (GA) required for proper cognitive functions. Using the retro-TRAP method, we characterized transcripts enriched in NGC neurons which have projections to the thalamus. The unique expression and activation of the endothelial nitric oxide (eNOS) signaling pathway in these cells and their intimate connections with blood vessels indicate that these neurons exert direct neurovascular coupling. Production of nitric oxide (NO) within eNOS-positive NGC neurons increases after environmental perturbations, indicating a role for eNOS/NO in modulating environmentally appropriate levels of GA. Inhibition of NO production causes dysregulated behavioral arousal after exposure to environmental perturbation. Further, our findings suggest interpretations for associations between psychiatric disorders and mutations in the eNOS locus.

nucleus gigantocellularis | endothelial nitric oxide synthase | reticular formation | thalamus | arousal

Are there unique molecular properties of the subtype of nucleus gigantocellularis (NGC) neurons with projections to central thalamus, cells crucial for maintaining CNS arousal? These neurons in the NGC of the reticular formation are capable of integrating information from virtually the entire CNS, as they feature extremely large dendritic arbors (1) and respond electrically to every sensory modality tested (2). Their ascending projections (3–6) provide excitatory inputs to central thalamic regions that are capable of supporting cortical activation and motor activity in animals (7, 8) and a patient in a vegetative state (9). Many NGC neurons have descending projections as well, reaching all levels of the spinal cord bilaterally. Here we provide a comprehensive analysis of those NGC neurons with long projections to the central thalamus.

Several lines of evidence indicate that these cells support a fundamental brain function known as “generalized arousal” (GA), crucial for initiation of all conscious movements (reviewed in refs. 6, 10, 11). Disorders of GA are involved in a variety of nervous system problems, including melancholic depression, bipolar disorders, attention deficit hyperactivity disorder, sleep problems, and disorders of consciousness (10). In addition, proper modulation of GA is essential for function in multiple cognitive tasks as described by the classical Yerkes–Dodson law (12–15).

Despite the crucial functional role of these neurons and their large size (40 μ m in a mouse; 100 μ m in humans), their extensive dendritic arbors and long axons complicate their isolation from adult animals. PCRs from single NGC neuronal mRNA obtained in slices of hindbrain from mouse pups showed that they can

express genes for receptors related to GA (11), but further transcriptome information was unavailable.

To address these challenges, we used a recently developed technique that allows the molecular characterization of particular neuronal subpopulations based on their neuroanatomical projections and the locations of their cell bodies (16, 17). This “retro-TRAP” (translating ribosome affinity purification from retrogradely labeled neurons) approach relies on viral injection into an anatomical area targeted by the neurons of interest, followed by selective precipitation of ribosomes from retrogradely labeled cell bodies, and subsequent RNA sequencing (RNA-seq) analysis (Fig. 14).

By comparing the mRNAs enriched in the NGC neurons which are retrogradely labeled due to viral injection into central thalamus with the gene expression of nonlabeled surrounding cells in NGC and then performing a comprehensive bioinformatics

Significance

Certain large neurons deep in the brainstem, in the nucleus gigantocellularis (NGC), are crucial for waking up the brain from deep sleep, anesthesia, or injury. NGC neurons, which project axons to central thalamus, should be especially important because central thalamic stimulation heightens CNS arousal in animals and in human patients. We have used the retroTRAP technique to discover mRNAs enriched in such NGC neurons. One mRNA, for endothelial nitric oxide synthase (eNOS), is uniquely expressed. By experiments both on the environmental/sensory side and with respect to motoric regulation, endothelial nitric oxide expression is shown to be functionally important. Five independent lines of evidence indicate that these eNOS neurons have a significant relation with their blood supply.

Author contributions: I.T., J.N.H.S., and D.W.P. designed research; I.T., M.F., M.A.D., T.A.M., R.L., R.R., T.M., J.N.H.S., and D.W.P. performed research; I.T., S.S., J.M.F., and J.N.H.S. contributed new reagents/analytic tools; I.T., Y.L., and M.H. analyzed data; and I.T., J.N.H.S., and D.W.P. wrote the paper.

Reviewers: M.-F.C., University of California, Los Angeles; and E.G.-R., University of Arkansas for Medical Sciences.

The authors declare no conflict of interest.

Published under the PNAS license.

Data deposition: The data reported in this paper have been deposited in the Gene Expression Omnibus (GEO) database (accession no. GSE115526).

¹To whom correspondence may be addressed. Email: itabansky@rockefeller.edu, Joel.n.h.stern@post.harvard.edu, or pfaff@rockefeller.edu.

²J.N.H.S. and D.W.P. contributed equally to this work.

This article contains supporting information online at www.pnas.org/lookup/suppl/doi:10.1073/pnas.1806123115/-DCSupplemental.

Published online July 2, 2018.

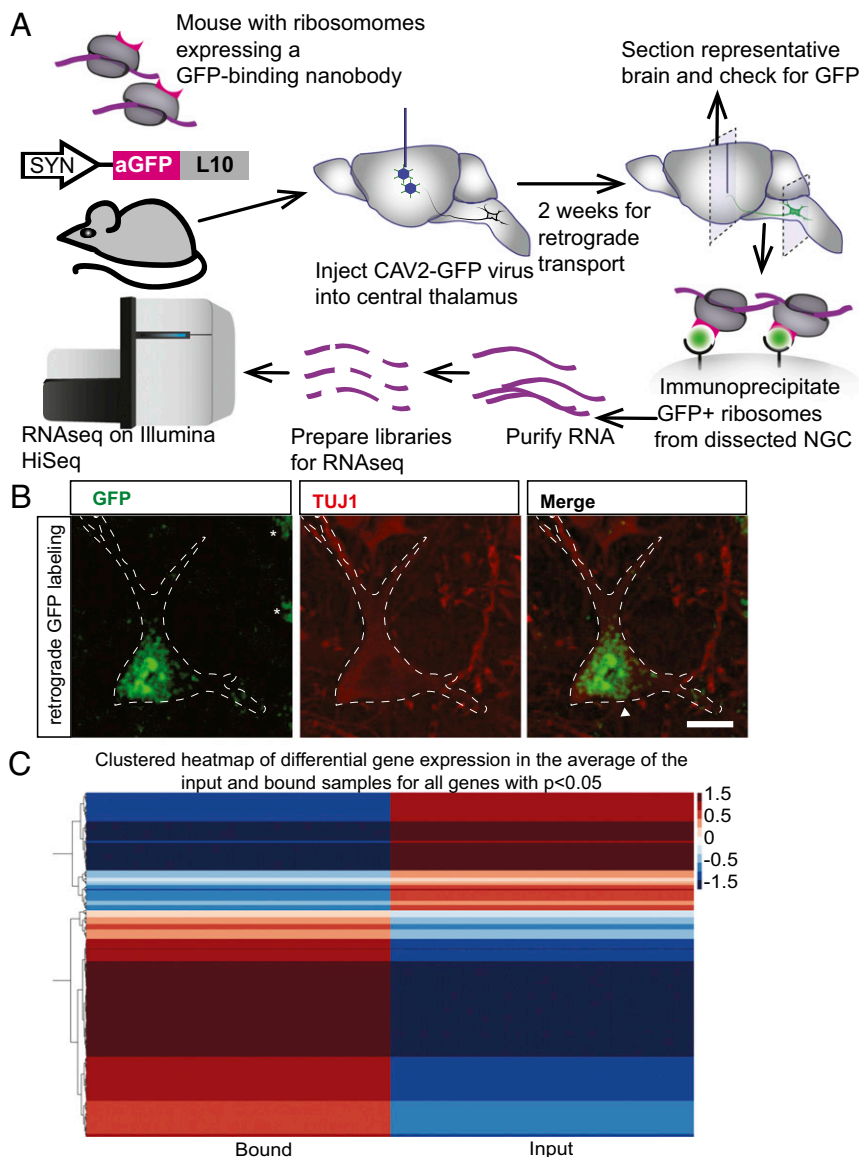


Fig. 1. Specific RNA-seq of NGC neurons with ascending projections. (A) Outline of the experimental procedure. CAV-GFP retrograde tracing virus was injected into the central thalamus of transgenic SYN-NB-L10 animals, which express the camelid nanobody against GFP fused to the L10 ribosomal subunit, under the control of the synuclein (SYN) promoter. Mice were allowed to recover for 2 wk after surgery to allow retrograde transport of the virus and then were killed. The NGC was dissected, and the GFP-labeled ribosomes were precipitated using magnetic beads coated with GFP antibody. The RNA from precipitated ribosomes (bound sample) and the total RNA from the NGC of the same animals (input sample) were sequenced on an Illumina HiSeq machine. (B) Viral injection into the central thalamus results in GFP expression in large NGC neurons. Shown are confocal micrographs of NGC neurons from virus-injected animals showing dim perinuclear GFP staining (green) consistent with GFP binding to ribosomes attached to the endoplasmic reticulum. TUJ1 (red) indicates neuronal-specific tubulin. Dashed white outlines indicate the shape of the labeled neurons. Asterisks indicate green neurons that are hidden behind projections from other cells. (Scale bar: 30 μ m.) (C) Heat map of all three experimental runs (biological replicates) showing all genes later found to be selectively up- or down-regulated ($P < 0.05$) in bound versus input samples. There were 339 genes observed to be selectively up- or down-regulated ($P < 0.05$) in the bound sample from NGC neurons compared with the input control. The heat map has been clustered to reveal groups of genes with similar patterns of expression.

analysis of these results, we were able to identify interesting candidate pathways important for these cells. This standard procedure allowed us to highlight genes and pathways that are unique to these neurons with projections ascending to thalamus compared with other cells in NGC.

The most surprising of these mRNAs enriched in NGC neurons with axons projecting to the thalamus was that for the endothelial nitric oxide synthase (eNOS) signaling pathway, which we verified by immunohistochemistry. Further behavior and histochemical experiments revealed a close physical proximity between the eNOS-positive neurons and the surrounding blood vessels (Fig. 2 C–E). Altogether, five independent lines of evidence—eNOS gene expression, pathway activation, immunohistochemistry, 3D reconstructions, and electron microscopy—show an unusual relation of these eNOS neurons to their vasculature.

Further, behavioral analysis combined with histochemistry indicated that the neurons show an increased amount of oxidative damage, indicative of nitric oxide (NO) production, after exposure to specific environmental perturbations. Finally, inhibition of NO synthesis specifically within the NGC indicates that this molecule plays a role in regulating behavioral arousal after environmental perturbations. In summary, our results show how these unusual giant neurons in the medullary reticular for-

mation contribute to the regulation of the elementary function GA by environmental changes.

Results

As soon as the results revealed the unique expression of eNOS (see below), we did several studies intended to explore the relation between this specific subset of NGC neurons, their vasculature, and NGC function.

RNA Labeling, Purification, and Detection of Enriched Transcripts in the Bound Sample. As the retro-TRAP approach has not been performed in the NGC before, we first tested whether we would be able to label the anterograde-projecting neurons from this area and isolate a sufficient quantity and quality of RNA from the labeled cells to detect enriched transcripts. Upon injection of a genetically modified canine adenovirus type 2 encoding GFP into the thalamus, retrograde GFP labeling was detected in large NGC neurons but not in vehicle-injected control brains. Notably, the GFP signal in labeled NGC neurons appeared to be stronger in the perinuclear region, suggesting that we successfully labeled ribosomes binding to the endoplasmic reticulum (Fig. 1 A and B and SI Appendix, Fig. S1).

We next tested whether we could selectively immunoprecipitate RNA of sufficient quality and quantity for RNA-seq from these labeled neurons. We were able to isolate sufficient quantities of RNA to perform three rounds of RNA-seq [>100 pg per run, RNA integrity numbers (RIN) >7], by pooling five or six animals per group.

For each of the three rounds of RNA-seq, we started with 100 pg of RNA, or more, and we obtained at least 20 million high-quality reads per sample. We then used a bioinformatics approach (*Methods*) to detect genes that were significantly up- or down-regulated in the bound sample (RNA isolated from ribosomes in retrogradely labeled NGC neurons) as opposed to the input sample (total RNA from this region of the brain). Alignment, pooling of samples, and adjusted P value calculations revealed 260 genes that were significantly up-regulated ($P < 0.05$) plus 79 genes that were significantly down-regulated when comparing the bound sample with the input sample (Fig. 1C).

In addition to transcripts expected to be differentially expressed in neurons (Fig. 2A and Dataset S1), we discovered the unique expression of *eNOS* and the components of the eNOS signaling pathway (Fig. 2B, confirmed by immunohistochemistry in Fig. 2C–E and discussed below). Thus, we succeeded in detecting genes and pathways enriched in NGC neurons retrogradely labeled by injection into the thalamus.

The majority of the neurons represented in the bound sample were glutaminergic, as indicated by the up-regulation of *Slc17a6* (*Vglut2*, vesicular glutamate transporter 2), a molecule that allows presynaptic neurons to target glutamate to synaptic vesicles (18).

Pathway Analysis of Genes Enriched Within the NGC Indicated Activation of Multiple Biochemical Pathways. The logical follow-up to the mRNA results is to explore which biochemical pathways would be expected to be up- or down-regulated in the labeled cells as compared with surrounding tissue. Pathway analysis with Ingenuity Pathway Analysis (IPA; Qiagen) found 38 canonical pathways which had z -scores either considerably greater or considerably lower than 0 and for which the up- or down-regulation was statistically significant. Some of these pathways were expected, such as synaptic long-term potentiation (LTP), while others were unexpected, such as thrombopoietin signaling. When pathways were broadly classified into groups based on physiological function, as described in prior reports from the IPA database, genes involved in neuronal function, cell size and survival, cell signaling, and endothelial function were observed to be overrepresented in our dataset. These groups are illustrated in Fig. 3 and are discussed further below.

To determine the activation state of the pathways in which the up-regulated genes discussed above might be involved, we performed a molecule activation prediction (MAP) analysis. This bioinformatics tool predicts the activation states of each pathway component based on the transcriptional state of the relevant genes. When all the pathways detected as having significant z -scores were analyzed, only three showed considerable activation in many parts of the pathway. These pathways included NO signaling in the cardiovascular system (discussed below and *SI Appendix, Fig. S2*), neuropathic pain signaling in dorsal horn neurons (*SI Appendix, Fig. S3*), and calcium signaling (*SI Appendix, Fig. S4*).

We were surprised by two of the pathways shown to be up-regulated by z -scores and MAP: NO signaling in endothelial cells and cardiac hypertrophy signaling. These pathways share expression of genes associated with eNOS, a molecule previously not reported in neurons within the intact brain. The enrichment of pathways related to blood vessel function combined with eNOS expression result from contamination of the bound sample by RNA from blood vessels surrounding the labeled cells. However, three aspects of our experiment made that source unlikely: (i) there was no detectable GFP labeling in blood vessels in the virus-injected mice; (ii) in the syn-NBL10 mice that we used, only neurons express ribosomes capable of binding GFP; and (iii) we used immunohistochemistry to confirm the

presence of eNOS in the cell membranes of multiple large NGC neurons (Fig. 2C–E). Thus, our detection of eNOS and other genes associated with blood vessels was unlikely to be entirely due to technical reasons. However, the question remains: Do the NGC neurons actually use eNOS to produce NO, or is the presence of this protein in the transcriptome due to other causes?

One reason to focus on eNOS and associated pathways was that they were some of the few shown to be consistently activated by MAP. Most other canonical pathways showed strong activation in some parts of the pathway but strong inhibition in other parts of the same pathway. These included LTP (*SI Appendix, Fig. S5*), actin cytoskeleton signaling (*SI Appendix, Fig. S6A*), ciliary-derived neurotrophic factor signaling (*SI Appendix, Fig. S6B*), cAMP-responsive element binding protein (CREB) signaling (*SI Appendix, Fig. S7*), and α -adrenergic signaling (*SI Appendix, Fig. S8B*). The adrenergic finding is especially notable, as many neurons within the regions express adrenergic receptors (*SI Appendix, Fig. S8A*).

Transcriptional Evidence for the Function of eNOS Within the NGC. As we had the transcriptome of the eNOS-expressing neurons in hand, our next question was whether the transcriptional signatures we detected in these neurons were consistent with their having the ability to activate eNOS. The eNOS protein can be activated by a large variety of factors, including ones relevant to GA, such as increases in intracellular calcium (such as occur during neuronal firing) (19), serotonin (20), and muscarinic acetylcholine receptors subtype M4 and M2 (21). In the bound sample, we observed enrichment of the serotonin receptor 5-HT₃ and the M4 muscarinic acetylcholine receptor as well as calcium-signaling pathways, suggesting that eNOS could be activated by these mechanisms.

To support the prediction that eNOS may be producing NO, we also observed enrichment of a gene required for NO production: *Slc7a1* [solute carrier family 7 member 1, also known as “mouse cationic transporter 1” (*MCAT1*)], a permease whose function is to transport cationic amino acids, including arginine—the substrate for NOS—into the cell (22, 23).

Evidence of a Close Relationship Between eNOS-Expressing Neurons and Local Vasculature. eNOS is usually present in blood vessels (19–21), and thus its presence and, potentially, its activity in a specific neuronal subtype was quite unexpected. We speculated that perhaps this molecule can be used to mediate cerebrovascular coupling in the NGC. To investigate our suspicions, we probed whether we could detect evidence of a relationship between the large NGC neurons and the surrounding cerebral microvasculature. When we used the retro-TRAP data to generate interaction networks, based on published curated literature, we also observed a network consisting entirely of extracellular matrix proteins, including collagens and integrins, as well as tyrosine kinase with Ig-like and EGF-like domains 1 [*Tie-1*, a receptor tyrosine kinase that is involved in stabilization of blood vessels (24)]. Other extracellular matrix proteins found in the vasculature and enriched in the bound sample include collagen type VI (25) and fibronectin (*Fnl*) (26). Likewise, integrin α 1 (*Itga1*), which was enriched in the bound sample, is part of a complex that mediates the interaction of endothelial cells with the extracellular matrix (27–29).

We therefore hypothesized that the production of these proteins by NGC neurons allows them to communicate more efficiently with blood vessels, either by inducing growth of the capillaries next to the neuronal cells or, conversely, by allowing them to bind to the capillary extracellular matrix using integrins. Electron microscopic images show that glutaminergic NGC neurons do indeed have their membranes apposed to endothelial cells (Fig. 2F and G).

In many areas of the brain, neurovascular coupling is mediated by astrocytes, which respond to neuronal activity by producing a variety of factors that cause vasodilation and a resultant increase in oxygen and glucose available to neurons (30). Our discovery of eNOS in NGC cells, combined with their close interactions with

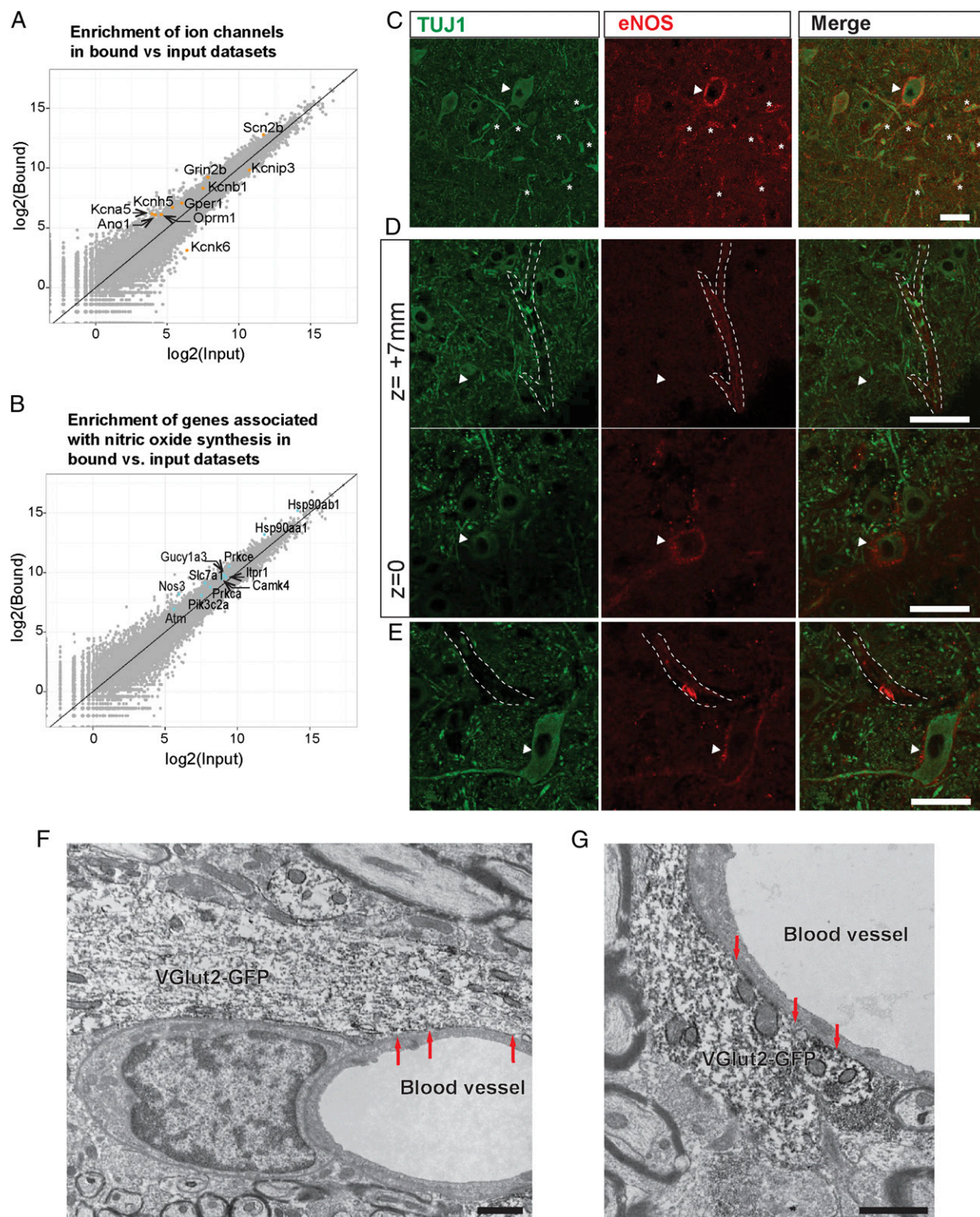


Fig. 2. Up-regulation of eNOS and proximity to blood vessels in NGC neurons. Box plots are intended to show all the data, and biologically significant points (fold change >2) are in color. Note that the axes for the box plots in A and B are log2. (A) Box plot of the most selectively expressed ion channel genes in the data sample. (B) Box plot of expression changes of selected genes related to the NO signaling pathway and its metabolic consequences. (C–E) TUJ1 (green) indicates neuronal-specific tubulin, DAPI (blue) stains nuclei, and eNOS is red. (Scale bars: 50 μ m.) (C) Confocal micrograph of an eNOS-positive NGC neuron showing expression in nearby process (asterisks) and in the cell body (arrowhead). TUJ1 (green) indicates neuronal-specific tubulin, and eNOS is shown in red. (D and E) A series of confocal optical sections showing the proximity of eNOS-positive neurons to putative blood vessels. (D) Two confocal optical sections showing an eNOS-positive neuron (arrowhead) located near a blood vessel (white outline). The *Upper Row* is 7 μ m above the *Lower Row* in the z plane. For example, regarding TUJ1, the cell body in the *Lower Row* is directly beneath the blood vessel outlined in the *Upper Row*. (E) A confocal optical section showing the proximity of an eNOS-positive neuron to a blood vessel. (F and G) Electron micrographs show NGC dendrites (identified using immunoperoxidase for anti-GFP antibody in vGlut2-GFP reporter mice) closely apposed to the basement membrane adjacent to the endothelial cells. (Scale bars: 500 nm.)

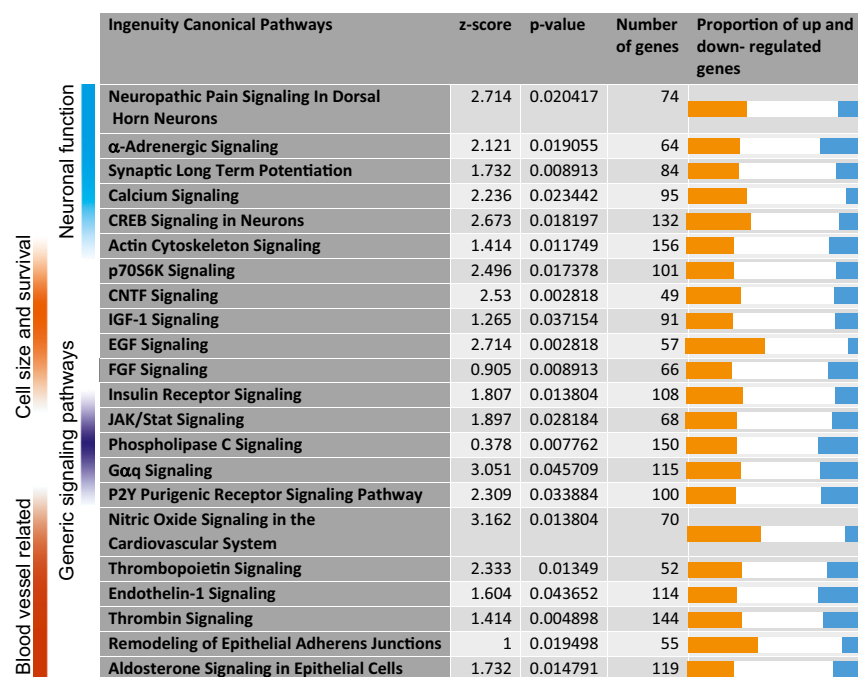


Fig. 3. The primary biological functions of signaling pathways up-regulated in NGC neurons. Plot of selected up-regulated canonical pathways with significant z-scores ($P < 0.05$) in bound versus input RNA samples, as defined by Ingenuity's core pathway analysis. These pathways fall into one of four categories: neuronal function, cell size and survival, signaling pathways, and interactions with blood vessels, as indicated by the colored bars on the left. Gradients in these bars indicate that they fulfill more than one function (for example, actin cytoskeleton signaling is involved in both neuronal function and cell size/survival). The plots on the right of the chart show the number of genes found to be up-regulated (orange), down-regulated (cyan), or unchanged (white) for each pathway.

the endothelial extracellular matrix, led us to infer that they are capable of contributing to the regulation of neurovascular coupling.

For eNOS in the NGC neurons to be able to influence the endothelium, the neuron itself must be in sufficient proximity to the blood vessel that the NO can signal to the endothelial cells. There is a large literature on the range of diffusion of NO in the brain, and it appears that 100 μm from its point of origin is an accurate, conservative estimate (31). Therefore, to have an effect on the vasculature (or the converse), the eNOS-positive NGC neurons would have to be less than 100 μm from blood vessels. The short diffusion range of NO suggests that, to have a systemic effect on the vasculature, it is necessary for the neurons to have multiple points of contact with the blood vessels. As NGC neurons have large dendritic trees, this possibility is not out of the question.

We therefore used immunohistochemistry and confocal microscopy to calculate the distance between eNOS-positive cell bodies and blood vessels in stained sections of the NGC with Imaris software (Bitplane). We also looked for eNOS staining in the projections of NGC neurons. We found eNOS expression in the cell membranes of a subpopulation of NGC neurons, and it marked a large number of projections within the NGC (Fig. 2C). Furthermore, even within the thin (20- μm) sections, we found that >90% eNOS-positive neuronal cell bodies were localized within 50 μm of blood vessels (Fig. 2D and E). 3D reconstructions of thicker sections (40 μm) indicated that a large number of eNOS-positive neurons have membranes closely apposed to blood vessels, and their projections also interact with blood vessels. This observation was confirmed by 3D reconstructions of confocal micrographs of eNOS-positive NGC neurons next to blood vessels (SI Appendix and Movies S1 and S2). Therefore it is likely that the NO produced by these cells has an influence on the surrounding blood vessels, and vice versa.

Thus, we have used five converging methodologies (eNOS gene-expression observations, immunohistochemical staining, pathway analyses, 3D reconstructions of confocal images, and electron microscopy) to support the inference that eNOS-positive NGC neurons have a close relationship to their blood supply.

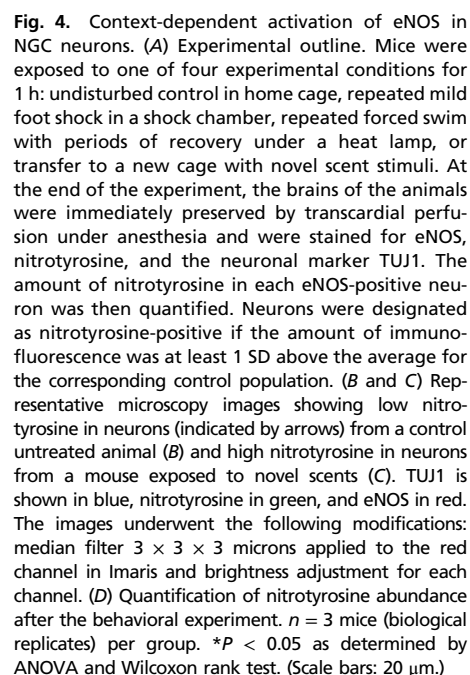
We then followed up these discoveries by functional experiments, first examining what inputs might activate eNOS and then studying the behavioral consequences of eNOS inhibition.

Function: ENOS Activation in the NGC Neurons Occurs in Response to Specific Perturbations in the Environment of the Mouse.

We next wanted to know whether eNOS within NGC neurons is activated in response to different environments. Knowing that the close proximity of eNOS-positive neurons to their blood supply would permit them to increase blood flow during periods of high activity, we hypothesized that eNOS activity would be dependent on NGC activation. NGC neurons have previously been documented to receive input from all sensory modalities; thus, if NO production is a result of neuronal activation, we should be able to detect eNOS activation in conditions that also increase GA. To test this hypothesis, we subjected the animals to different environments (Fig. 4A) and monitored the activation of eNOS-positive neurons by quantifying nitrotyrosine, a well-documented protein modification that occurs as a result of NO production, in eNOS-positive cell bodies within the NGC (32–34).

To increase GA, we performed three environmental perturbations: (i) exposure of the animal to a clean cage containing novel scents with which it is able to interact for 1 h; (ii) transferring the animal to a shock chamber and delivering 15 mild, unpredictable foot shocks for 1 h; or (iii) three repeated bouts of forced swim, followed by periods of recovery under a heat lamp to prevent hypothermia. Unperturbed animals in the home cage served as controls. In all cases, the brains of the animals were collected for analysis immediately following the treatment.

We initially expected that GA would increase more as a result of stress and that high-stress conditions, such as a foot shock or forced swim, would cause higher levels of nitrotyrosine to be observed. We did indeed find that the overall amount of nitrotyrosine in the neurons staining positive for eNOS was quite low in control animals and that it was increased in certain experimental animals. However, the foot-shock condition, which has been documented extensively in the literature to be quite stressful (35, 36), did not result in a statistically significant increase in the amount of nitrotyrosine within eNOS-positive neurons in the NGC. In contrast, both exposure to novel scents and the forced swim test resulted in large, statistically significant increases in the amount of nitrotyrosine observed within these cell bodies (Fig. 4B–D). Thus, the NGC neurons appeared to produce NO only in particular circumstances. However, it was still unclear whether NO production within the NGC produces an effect on GA; this requires the output of the GA system to be measured, as we did in the following experiments.



To determine a behavioral role of NO derived from eNOS in NGC function, we sought to inhibit NO production within the NGC in awake and behaving animals. As no eNOS-knockout mice are available that are specific to this region, we instead opted for chemical inhibition by implanting cannulae that allow

We implanted the cannula after the month of recording the baseline daily activity levels of each animal. Once the mice had recovered, their motor coordination (using the rotarod) and basal levels of activity were assessed. No significant motor impairments or changes in daily activity were observed postsurgery (Fig. 5*D*).

We next used the implanted cannula to introduce either saline or L-NAME into the NGC of the experimental animals (this required a <5-min period of handling per mouse). The mice were then placed in a new cage containing unfamiliar scent stimuli for 1 h. At the end of the stimulus period, the animals were then placed back into their home cages and were allowed to recover. The activity of the mice was monitored continuously from the start of the experiment until 3 d postinjection.

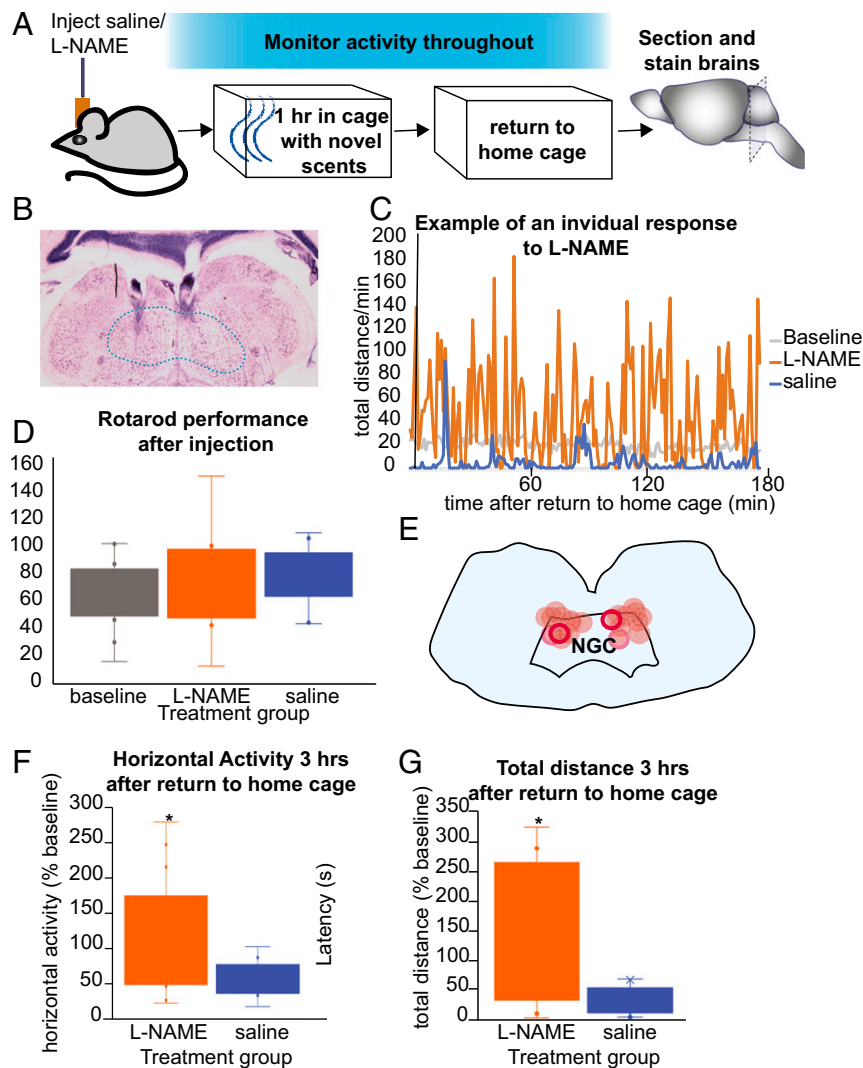


Fig. 5. Inhibition of eNOS causes dysregulation of behavioral arousal after exposure to novel stimuli. (A) Outline of the experiment. Cannulated mice were first injected with either the eNOS inhibitor L-NAME or vehicle (saline). They were then introduced into a new cage with scent stimuli in an isolated, controlled environment and were allowed to explore freely. After 1 h they were returned into the home cage. Their activity was monitored throughout. The animals were allowed to recover for 3 d before the experiment was repeated with the injection of the other compound (L-NAME if they initially had received saline and saline if they initially had received L-NAME) and a different set of novel stimuli. Thus, each animal served as its own control. After completion of the experiment, cannulae placements were confirmed by histology. (B) Histological placement of the cannulae in mouse M7, as indicated by the glial scarring. The NGC is indicated by a dashed blue line. (Magnification: 40 \times .) (C) Example of a strong response to L-NAME, showing extreme, repeated fluctuations of activity. Total distance traveled in the 3 h after return to the home cage (binned by minute) for mouse M7, showing the baseline activity (unperturbed in home cage, averaged over the period of 1 mo) in gray, the activity level after saline injection in blue, and the activity level after L-NAME in orange. (D) Motor coordination is not altered by the L-NAME injection. Latency to falling off the rotarod for mice without injection (gray), injected with L-NAME (orange), or injected with saline (blue). $n = 9$ animals. (E) Summary of all cannulae placements in the mice included in the dataset. The placement of each cannula on each side is shown in orange. The red circles indicate mouse M7. The outline of the brainstem is derived from the Paxinos online atlas (59). (F and G) Animals treated with L-NAME show much higher activity after exposure to novel stimuli than animals treated with saline. Graphs show average baseline-adjusted horizontal activity (F) and total distance travelled (G) for 3 h after return to the home cage. $n = 11$ animals per group. $*P < 0.02$ by paired t test.

At the end of the 3-d recovery period, the mice were microinjected with L-NAME if they received saline during the first test, and vice versa, and the procedure was repeated with novel scent stimuli (different from those used in the initial test) (Fig. 5A). Thus, each animal served as its own control for each round of experiments. We did not observe a significant effect of the type of stimuli used or the order in which the compounds were tested on the results of the experiment.

At the end of the experiment, the effect of L-NAME on motor coordination was assessed using the rotarod. For the rotarod experiment, each animal was again randomly assigned to receive either saline or L-NAME and then was allowed to recover for 3 d; the experiment was repeated with the other compound. No

effect of L-NAME administration on motor coordination was observed (Fig. 5D).

While we initially expected eNOS inhibition to decrease GA, because we would be downregulating a normal molecular reaction in neurons known to increase GA, initial comparisons of the activity levels of each treatment group (microinjected with saline or L-NAME) showed no significant difference in the reaction to the unfamiliar scent stimulus. Both treatment groups showed increased levels of activity, 176% of baseline on average, compared with their normal activity at that particular time of day. The increase in activity was observable both when we analyzed total distance traveled within the assay apparatus and when

we analyzed smaller, fidgeting movements resulting in single horizontal beam breaks within the apparatus (Fig. 5 *F* and *G*).

However, there was a striking difference in activity after the animals returned to the home cage. The animals treated with saline showed a notable decrease in activity, with the total distance traveled within the cage being 64% of their baseline activity. This is consistent with recovery after a highly stimulating event. In contrast, the average activity levels in animals treated with L-NAME remained elevated, with the total distance traveled in the cage being 164% of baseline. This difference was statistically significant when both fidgeting behavior (horizontal activity) and total distance traveled within the cage were analyzed ($n = 11$ mice, $P < 0.02$ for both measures). This overall increase resulted from a decrease in the amount of time spent at rest and also from increased locomotor speed and frequency of moving about in the cage. Under normal conditions, animals produce bursts of activity that look like spikes. In animals treated with L-NAME, both the frequency and the amplitude of the spikes were considerably increased.

Notably, this effect showed high individual variability and was observed only in animals in which histological placement confirmed that the cannula ended within the NGC. No change in activity was noted in animals in which the cannula was implanted just outside the NGC, ($n = 3$). Similarly, no difference between saline and L-NAME treatment was detectable in animals that had not been previously exposed to novel stimuli ($n = 6$).

The most robust response was in the animals that received injections into the dorsal posterior NGC, consistent with an immunohistochemical observation of intensely staining eNOS-positive neurons located in that region as well as more laterally within the NGC. However, the location of cannula implantation varied from animal to animal, which could account for the variability observed in the responses to L-NAME (Fig. 5*E*).

The results from these two sets of functional experiments—eNOS activation and eNOS inhibition—indicated that NO production from eNOS-expressing neurons in the NGC occurs in response to specific environmental perturbations and that it is needed to stabilize GA levels once the animal returns toward a resting state.

Discussion

The surprising results of the project have implications for the regulation of arousal and also have potential clinical links. Since the retroTRAP methodology was developed quite recently, we first examine the properties of our approach for isolating RNA from NGC neurons.

Technical Considerations. Here we present transcriptome data on a vital subpopulation of giant neurons which are involved in the regulation of GA and whose axonal trees include projections to the thalamus. Most surprising, we have uncovered a function for eNOS-expressing NGC neurons in regulating arousal (3–6, 8, 9). In describing this subpopulation, we pushed the limits of the retro-TRAP technique (16), identifying cell bodies that are more than 1 cm away from the injection site. GFP expression in labeled cells could be detected only by antibody staining (Fig. 1*B*), a potential technical advantage, as it reduces the proportion of GFP that is unbound to ribosomes during lysis, which in turn decreases the probability of nonspecific purification of RNA from cells outside the targeted population.

Technologies involving TRAP have become powerful tools for analyzing the gene-expression patterns of different neuronal subpopulations. However, the very nature of the technique is based on the enrichment of ribosome-bound RNA using affinity purification (Fig. 1*A*). In contrast, the standard control used in these techniques is total RNA from the surrounding brain region (in our case, the input). This means that enrichment of a particular RNA in the bound sample can occur either through increased transcription of the RNA in the target population or by an increased probability of its binding to ribosomes. Either mechanism would indicate increased translation of this particular RNA. Due

to ribosome purification, the detection of untranslated RNAs, such as microRNAs, is possible but less likely to occur.

Implications of the Results. The results of our experiments point to several surprising features of large NGC neurons. Our combined observations of the enrichment of molecules related to the function of blood vessels in these cells (Figs. 3 and 4) and their proximity to capillaries (Fig. 2 *C* and *D*) suggest that these neurons may crosstalk with the endothelial cells to regulate their own blood supply, a role that is generally thought to be filled by glia (30, 39).

The functional and behavioral results supported by the NGC neuronal transcriptome have both a sensory side (Fig. 4) and a motor side (Fig. 5). Regarding sensory inputs, we show the sensitivity of eNOS-expressing NGC neurons to environmental perturbation, which results in the production of NO (Fig. 4). Regarding motor output, we report significant changes in two forms of activity when NO production is inhibited (Fig. 5). This change in activity occurs only after prior exposure to novelty, indicating context dependence.

Our gene-expression assays indicate that the GA-related transmitters serotonin and acetylcholine can activate NO production in these neurons, as both are capable of inducing NO production by eNOS (20, 21). RNA encoding both muscarinic cholinergic and serotonin receptors are enriched in our bound sample (Dataset S1). There are cholinergic afferents as well; a strong candidate for this action is the pedunculopontine tegmental nucleus and the lateral tegmental nucleus. These brainstem nuclei are important parts of CNS arousal systems (40) and contain cholinergic cell populations which project to the reticular formation (41). Likewise, serotonin is also strongly produced in the brainstem raphe nuclei, and detailed analyses of its source and mechanism of action within the raphe nuclei adjacent to the NGC are warranted in future studies.

Clinical Links. The present observations led to links between these unique NGC neurons and a variety of studies that, unexpectedly, suggested an important role for eNOS in higher brain functions (38, 42–51). L-NAME injections and NOS knockout have been shown to alter mouse behavior (38, 42–44). In the case of the NGC specifically, the mice injected with an eNOS inhibitor show a decrease in resting time and an increase in the speed of locomotion after exposure to novel scents and return to the home cage. The NGC has previously been linked to habituation (2), and it is possible that the eNOS expression and activation patterns that we observed are involved in environmental adaptation. An inability to adjust one's reactions to one's surrounding could have a variety of adverse clinical and subclinical effects.

Consistent with the above comments, multiple studies have implicated polymorphisms in the NOS-III (*eNOS*) gene in humans in various aspects of bipolar and major depressive disorder, including suicidality (45–51). While the effects of NOS-III mutations on cerebral vascular perfusion and neurogenesis likely play a role in the etiology of these disorders, it is likely that the direct impacts of eNOS function on GA provide an additional mechanism for how NOS-III mutations contribute to the development of these psychiatric problems. As we suspect a role for eNOS in neurovascular coupling, it is possible that these mutations alter the communication between NGC neurons and the surrounding vasculature, possibly in a manner somewhat phenocopied by the L-NAME experiments. The signaling pathways associated with eNOS would be disrupted in the long term, potentially causing difficulties with adaptation to long-term stress or environments that cause prolonged high levels of GA. The result would be a decrease in resilience to environmental perturbation that could, in the long term, lead to adverse psychiatric symptoms.

Methods

Animals. Experiments on animals were approved by the Rockefeller University Animal Care and Use Committee. Syn-NB-L10 mice were generated in the J.M.F. laboratory and were backcrossed to C57BL/6J mice as heterozygotes.

All animals were group housed in standard shoebox cages with food and water ad libitum. Animals were genotyped at weaning with the following primers: forward: GCG GCT ACC CCT ACG ACG TT and reverse: TGG TGA ATC GGC CCT TCA CGG. Virus injection experiments, which proceeded in three independent runs, were performed in 8- to 16-wk-old animals. For retro-TRAP, each experimental group contained five or six animals, including two to four females. C57BL/6J mice were purchased from Jackson Laboratories and bred in the laboratory for three generations. They were killed for tissue harvest at 12–20 wk of age. VGlut2-GFP mice [stock Tg(Slc17a6-EGFP)FY115Gsat/Mmud] were obtained from GenSat.

Retrograde Viral Labeling. Mice were anesthetized with isoflurane in 100% oxygen and were placed in the ear bars. A Hamilton syringe containing 1 μ L of canine adenovirus (CAV)-GFP was lowered into the midbrain at \sim 1.2 mm anteroposterior (AP), \pm 1 mm mediolateral (ML), and 5 mm dorsoventral (DV) (*SI Appendix, SI Methods*). After recovery, animals were housed in biosafety level 2 cages for 2 wk to allow retrograde transport. After 2 wk, animals were killed for immunohistochemistry and RNA isolation (see below).

RNA Isolation and Sequencing. RNA isolation for retro-TRAP was performed as previously described (16). RNA quality was evaluated using an Agilent Bioanalyzer system. Sequencing was performed on an Illumina HiSeq machine.

Immunohistochemistry. Mice were transcardially perfused with ice-cold PBS followed by 4% paraformaldehyde (PFA) under deep anesthesia (0.8 mg/kg ketamine and 0.12 mg/kg xylazine). Brains were dissected and postfixed in 4% PFA for 8–16 h. Brains were sectioned on a Leica vibratome at 60–80 μ m thick or on a sledge microtome at 20–40 μ m thick. For antibodies and the detailed immunohistochemistry protocol, please see *SI Appendix, SI Methods*. Controls for immunohistochemistry included brain regions where protein expression was not expected (based on existing data), no primary, and staining brain regions/structures where staining would be expected (e.g., cerebral blood vessels for eNOS). Additionally, for nitrotyrosine, multiple monoclonal antibodies from different vendors were used to confirm the consistency of staining.

Labeling the Blood–Brain Barrier. Labeling with EZ-Link Sulfo-NHS-Biotin (Thermo Fisher) was added to the PBS at a concentration of 1 mg/mL, and the mouse was transcardially perfused for 3 min before a 5-min perfusion with PFA. The tissues were processed as described above (see *Immunohistochemistry* above).

Electron Microscopy. The brains of GluN1-EGFP mice were prepared for electron microscopic studies using previously described methods (see *SI Appendix, SI Methods* for more information) (52). Profiles containing GFP immunoreactivity were classified as neuronal (soma, dendrites, axons, terminals) or glial based on criteria previously described (53).

Environmental Perturbation Experiments for Measuring Nitrotyrosine. Mice for environmental perturbation experiments were 8- to 12-wk-old males of a C57BL/6J background. Mice were group-housed continuously before the start of the experiment. For the experiment, mice were transferred to a new cage containing a spoonful of coffee, a spoonful of rosemary, five roasted unsalted pistachios, and a spoonful of cinnamon in each corner of the cage (for novel scents), or were placed in room-temperature water in a clear glass cylinder for periods of 15, 10, and 5 min, followed by recovery under a heat lamp in a clean cage for 20 and 15 min, or were placed in a shock chamber and administered mild foot shocks for 1 h at unpredictable intervals but no more frequently than 1 every 5 min, or were left unperturbed as controls. All perturbations were conducted during the second part of the dark phase of the day/night cycle. Mice were all monitored continuously for signs of distress. Following the experiments, mice were killed immediately by transcardial perfusion under ketamine/xylazine anesthesia. Their brains were postfixed for 12 h in PFA and processed for staining as described.

Image Processing and Analysis. Image analysis was performed using Imaris software (v5.1; Bitplane). A 3×3 median filter was used to remove noise on the red (eNOS) channels for better detection of eNOS neurons. The maximum cutoff was adjusted to increase detection of eNOS-positive neurons. No filters or brightness adjustments were performed on nitrotyrosine staining, as it was the parameter being quantified.

For nitrotyrosine staining, quantification of secondary immunofluorescence is inherently problematic due to the amplification of signal by the secondary antibody. To avoid this problem, we used a high concentration of

primary antibody (1:200) and few brain sections per staining to achieve antibody saturation. We further addressed this issue by calling nitrotyrosine-positive only those neurons that were at least 1 SD above average in fluorescence intensity, thus accounting for potential variability in antibody staining.

Cannulation. Mice used in the experiment were adult (3- to 6-mo-old) male littermates from a C57BL/6J background. For the duration of the experiment, mice were housed individually, with normal chow diet (no.5053) and water ad libitum.

The home-cage activity of each experimental animal was recorded for 1 mo, producing a baseline for daily activity. Mice were measured continuously for ambulatory activity using a VersaMax Animal Activity Monitoring System (AccuScan Instruments, Inc.) with a sample interval duration of 60 s and a light/dark cycle of 12 h with lights on at 3 AM and lights off at 3 PM. Data were collected and analyzed using the VersaMax Analyzer and VersaDat software (AccuScan Instruments, Inc.), respectively.

Mice received i.p. injections of 2 mg/kg flunixin meglumine (Banamine) 30 min before surgery and then every 24 h for 3 d. Surgical anesthesia was isoflurane in O₂ (for more details, see *SI Appendix, SI Methods*). They were implanted with a double-guide cannula (5-mm length, 26 gauge, 1-mm distance between the cannulae; Plastics One Inc.) containing a dummy cannula of equal length (for details, see *SI Appendix, SI Methods*). Mice were placed back into their home cage and under infrared light for 30 min for postoperative monitoring.

Rotarod and Activity Measurements of Cannulated Mice. All injections (INJ1–4) took place within the first hour of the dark cycle, with at least 72 h of recovery time between injections and a maximum of four injections per animal. Using double internal cannulae (30 gauge, 5-mm length; Plastics One Inc.) that were connected to Hamilton syringes (model 7001; Hamilton Company) via water-filled polyethylene tubes (no. 51158; Stoelting), we injected mice with 0.5 μ L per side of either the NOS inhibitor L-NAME (ab120136; Abcam; 100 mM in 0.9% normal saline) or with vehicle only in a randomized manner; in the subsequent injection, mice initially injected with L-NAME would be injected with vehicle, and vice versa. In INJ1 and INJ2, the mice were placed into a new cage box that contained two novel olfactory stimuli; these were coffee powder and pistachios after INJ1 and cinnamon powder and dried rosemary leaves after INJ2. This was followed by an undisturbed recording period of 1 h in the novel cage, followed by 24-h recording in the home cage. In INJ3 and INJ4, the mice were again injected with L-NAME or saline, followed by a 10-min rest period and a rotarod assay.

Mice were trained for the rotarod (Panlab/Harvard Apparatus) 24 h before the first rotarod assay, until they reached a latency before falling of at least 5 min at 4 rpm. The rotarod assays were performed 24 h before surgery, 24 h before the first injection experiment, and after INJ3 and INJ4. Each assay consisted of three trials per mouse, with resting periods of 5 min between trials. The average of the three latency measurements (in seconds) was used for analysis.

Quantification and Statistical Analysis. For RNA-seq, quality assessment and pathway analyses were performed using conventionally accepted software. RIN scores were obtained using an Agilent Bioanalyzer. The fastq files were generated through CASAVA v1.8.2 (Illumina). They were then examined using the qualimap application (54) to make sure all samples were sequenced with proper quality. Reads were first trimmed by cutadapt v1.83 with the following parameters: cutadapt-times = 2-quality-base = 33-quality-cutoff = 5 –a AAAAAAAAAAAAAA –a TTTTTTTTTTTTTT –a AGATCGGAAGAG –a CTCCTCCGATCT. Trimmed reads were then aligned to mm10 using STAR v2.4.2a (55) aligner with default parameters. The alignment results were evaluated through RNA-SeQC v1.17 (56) to make sure all the samples had a consistent alignment rate and no obvious 5' or 3' bias. Aligned reads were then summarized through feature counts (57) with the gene model from Ensemble at gene level. DESeq2 (58) was used for gene differential expression analysis. Significantly changed genes were called by applying the following filtering: log2 fold change >1 and padj <0.05. Pathway analysis was done through Ingenuity IPA version 01-07 (Qiagen) on genes with a fold change >2 and padj <0.05.

For behavioral data all data analysis was carried out using Microsoft Office Excel 2016 (see *SI Appendix, SI Methods* for details of data analysis).

Data and Software Availability. The RNA-seq data have been deposited in the GEO database (accession no. GSE115526).

Additional Resources. Qualimap is available at doi: 10.1093/bioinformatics/bts503.

ACKNOWLEDGMENTS. We thank the Rockefeller Genomics Resource Center for technical support on sequencing; the Rockefeller University Bioimaging Resource Center for microscopes; Imaris for data analysis; Kaye Thomas and Tao Tong for technical assistance; Hazel Szeto for consultations on the data;

Rae Silver for a critical reading and feedback on the manuscript; and Nadera Rahman for assistance with the surgeries. I.T. was supported by NIH Grant F32 HD081835 and the New York Neuroscience Foundation. J.N.H.S. was supported by an HF Langbert Neuroimmunology Research Award.

- Ramón-Moliner E, Nauta WJ (1966) The isodendritic core of the brain stem. *J Comp Neurol* 126:311–335.
- Martin EM, Pavlides C, Pfaff D (2010) Multimodal sensory responses of nucleus reticularis gigantocellularis and the responses' relation to cortical and motor activation. *J Neurophysiol* 103:2326–2338.
- Jones BE, Yang TZ (1985) The efferent projections from the reticular formation and the locus coeruleus studied by anterograde and retrograde axonal transport in the rat. *J Comp Neurol* 242:56–92.
- Vertes RP, Martin GF, Waltzer R (1986) An autoradiographic analysis of ascending projections from the medullary reticular formation in the rat. *Neuroscience* 19: 873–898.
- Zemlan FP, Behbehani MM, Beckstead RM (1984) Ascending and descending projections from nucleus reticularis magnocellularis and nucleus reticularis gigantocellularis: An autoradiographic and horseradish peroxidase study in the rat. *Brain Res* 292: 207–220.
- Pfaff DW, Martin EM, Faber D (2012) Origins of arousal: Roles for medullary reticular neurons. *Trends Neurosci* 35:468–476.
- Wu HB, Stavarache M, Pfaff DW, Kow LM (2007) Arousal of cerebral cortex electroencephalogram consequent to high-frequency stimulation of ventral medullary reticular formation. *Proc Natl Acad Sci USA* 104:18292–18296.
- Tabansky I, et al. (2014) Temporally-patterned deep brain stimulation in a mouse model of multiple traumatic brain injury. *Behav Brain Res* 273:123–132.
- Schiff ND, et al. (2007) Behavioural improvements with thalamic stimulation after severe traumatic brain injury. *Nature* 448:600–603, and erratum (2008) 452:120.
- Pfaff DW (2006) *Brain Arousal and Information Theory: Neural and Genetic Mechanisms* (Harvard Univ Press, Cambridge, MA), pp vi, 205.
- Martin EM, et al. (2011) Molecular and neuroanatomical characterization of single neurons in the mouse medullary gigantocellular reticular nucleus. *J Comp Neurol* 519: 2574–2593.
- Yerkes RM, Dodson JD (1908) The relation of strength of stimulus to rapidity of habit-formation. *J Comp Neurol* 18:459–482.
- Gao XB, Horvath T (2014) Function and dysfunction of hypocretin/orexin: An energetic point of view. *Annu Rev Neurosci* 37:101–116.
- Zhu Y, Zhao Y, Ybarra O, Stephan WG, Yang Q (2015) Enhanced memory for both threat and neutral information under conditions of intergroup threat. *Front Psychol* 6:1759.
- Wang Z, et al. (2015) Is math anxiety always bad for math learning? The role of math motivation. *Psychol Sci* 26:1863–1876.
- Ekstrand MI, et al. (2014) Molecular profiling of neurons based on connectivity. *Cell* 157:1230–1242.
- Nectow AR, Ekstrand MI, Friedman JM (2015) Molecular characterization of neuronal cell types based on patterns of projection with Retro-TRAP. *Nat Protoc* 10:1319–1327.
- Takamori S, Rhee JS, Rosenmund C, Jahn R (2001) Identification of differentiation-associated brain-specific phosphate transporter as a second vesicular glutamate transporter (VGLUT2). *J Neurosci* 21:RC182.
- Presta A, Liu J, Sessa WC, Stuehr DJ (1997) Substrate binding and calmodulin binding to endothelial nitric oxide synthase coregulate its enzymatic activity. *Nitric Oxide* 1: 74–87.
- McDuffie JE, Coaxum SD, Maleque MA (1999) 5-hydroxytryptamine evokes endothelial nitric oxide synthase activation in bovine aortic endothelial cell cultures. *Proc Soc Exp Biol Med* 221:386–390.
- Waid DK, Chell M, El-Fakahany EE (2000) M(2) and M(4) muscarinic receptor subtypes couple to activation of endothelial nitric oxide synthase. *Pharmacology* 61:37–42.
- Kim JW, Closs EI, Albritton LM, Cunningham JM (1991) Transport of cationic amino acids by the mouse ecotropic retrovirus receptor. *Nature* 352:725–728.
- Palmer RM, Ashton DS, Moncada S (1988) Vascular endothelial cells synthesize nitric oxide from L-arginine. *Nature* 333:664–666.
- Sato TN, et al. (1995) Distinct roles of the receptor tyrosine kinases Tie-1 and Tie-2 in blood vessel formation. *Nature* 376:70–74.
- Kuo HJ, Maslen CL, Keene DR, Glanville RW (1997) Type VI collagen anchors endothelial basement membranes by interacting with type IV collagen. *J Biol Chem* 272: 26522–26529.
- Courtroy PJ, Boyles J (1983) Fibronectin in the microvasculature: Localization in the pericyte-endothelial interstitium. *J Ultrastruct Res* 83:258–273.
- Senger DR, et al. (2002) The alpha(1)beta(1) and alpha(2)beta(1) integrins provide critical support for vascular endothelial growth factor signaling, endothelial cell migration, and tumor angiogenesis. *Am J Pathol* 160:195–204.
- Senger DR, et al. (1997) Angiogenesis promoted by vascular endothelial growth factor: Regulation through alpha1beta1 and alpha2beta1 integrins. *Proc Natl Acad Sci USA* 94:13612–13617.
- Davis GE, Senger DR (2005) Endothelial extracellular matrix: Biosynthesis, remodeling, and functions during vascular morphogenesis and neovessel stabilization. *Circ Res* 97: 1093–1107.
- Muoio V, Persson PB, Sendeski MM (2014) The neurovascular unit—Concept review. *Acta Physiol (Oxf)* 210:790–798.
- Ledo A, Frade J, Barbosa RM, Laranjinha J (2004) Nitric oxide in brain: Diffusion, targets and concentration dynamics in hippocampal subregions. *Mol Aspects Med* 25: 75–89.
- Van der Vliet A, et al. (1994) Interactions of peroxynitrite with human plasma and its constituents: Oxidative damage and antioxidant depletion. *Biochem J* 303:295–301.
- Gow AJ, Duran D, Malcolm S, Ischiropoulos H (1996) Effects of peroxynitrite-induced protein modifications on tyrosine phosphorylation and degradation. *FEBS Lett* 385: 63–66.
- Ischiropoulos H, et al. (1992) Peroxynitrite-mediated tyrosine nitration catalyzed by superoxide dismutase. *Arch Biochem Biophys* 298:431–437.
- Stone EA, Freedman LS, Morgano LE (1978) Brain and adrenal tyrosine hydroxylase activity after chronic footshock stress. *Pharmacol Biochem Behav* 9:551–553.
- Ong LK, et al. (2014) Neurobiological consequences of acute footshock stress: Effects on tyrosine hydroxylase phosphorylation and activation in the rat brain and adrenal medulla. *J Neurochem* 128:547–560.
- Wong ML, et al. (1996) Inducible nitric oxide synthase gene expression in the brain during systemic inflammation. *Nat Med* 2:581–584.
- Haley JE, Wilcox GL, Chapman PF (1992) The role of nitric oxide in hippocampal long-term potentiation. *Neuron* 8:211–216.
- Filosa JA, Iddings JA (2013) Astrocyte regulation of cerebral vascular tone. *Am J Physiol Heart Circ Physiol* 305:H609–H619.
- Garcia-Rill E (2015) *Waking and the Reticular Activating System in Health and Disease* (Elsevier, Boston).
- Jones BE (1990) Immunohistochemical study of choline acetyltransferase-immunoreactive processes and cells innervating the pontomedullary reticular formation in the rat. *J Comp Neurol* 295:485–514.
- Frisch C, et al. (2000) Superior water maze performance and increase in fear-related behavior in the endothelial nitric oxide synthase-deficient mouse together with monoamine changes in cerebellum and ventral striatum. *J Neurosci* 20:6694–6700.
- Haul S, Gödecke A, Schrader J, Haas HL, Luhmann HJ (1999) Impairment of neocortical long-term potentiation in mice deficient of endothelial nitric oxide synthase. *J Neurophysiol* 81:494–497.
- Son H, et al. (1996) Long-term potentiation is reduced in mice that are doubly mutant in endothelial and neuronal nitric oxide synthase. *Cell* 87:1015–1023.
- Comings DE, et al. (2000) Multivariate analysis of associations of 42 genes in ADHD, ODD and conduct disorder. *Clin Genet* 58:31–40.
- Reif A, et al. (2006) A NOS-III haplotype that includes functional polymorphisms is associated with bipolar disorder. *Int J Neuropsychopharmacol* 9:13–20.
- Okochi T, et al. (2011) Genetic association analysis of NOS3 and methamphetamine-induced psychosis among Japanese. *Curr Neuropsychopharmacol* 9:151–154.
- Oliveira J, et al. (2015) Violent suicidal behaviour in bipolar disorder is associated with nitric oxide synthase 3 gene polymorphism. *Acta Psychiatr Scand* 132:218–225.
- Kittel-Schneider S, et al. (2015) Multi-level biomarker analysis of nitric oxide synthase isoforms in bipolar disorder and adult ADHD. *J Psychopharmacol* 29:31–38.
- Kawohl W, et al. (2008) Association of functional polymorphisms in NOS1 and NOS3 with loudness dependence of auditory evoked potentials. *Int J Neuropsychopharmacol* 11: 477–483.
- Rujescu D, et al. (2008) NOS-I and -III gene variants are differentially associated with facets of suicidal behavior and aggression-related traits. *Am J Med Genet B Neuropsychiatr Genet* 147B:42–48.
- Milner TA, Waters EM, Robinson DC, Pierce JP (2011) Degenerating processes identified by electron microscopic immunocytochemical methods. *Methods Mol Biol* 793: 23–59.
- Peters A, Palay SL, Webster Hd (1976) *The Fine Structure of the Nervous System: Neurons and Their Supporting Cells* (W. B. Saunders Co., Philadelphia), 3rd Ed, pp xviii, 494.
- García-Alcalde F, et al. (2012) Qualimap: Evaluating next-generation sequencing alignment data. *Bioinformatics* 28:2678–2679.
- Dobin A, et al. (2013) STAR: Ultrafast universal RNA-seq aligner. *Bioinformatics* 29: 15–21.
- DeLuca DS, et al. (2012) RNA-SeQC: RNA-seq metrics for quality control and process optimization. *Bioinformatics* 28:1530–1532.
- Liao Y, Smyth GK, Shi W (2014) featureCounts: An efficient general purpose program for assigning sequence reads to genomic features. *Bioinformatics* 30:923–930.
- Love MI, Huber W, Anders S (2014) Moderated estimation of fold change and dispersion for RNA-seq data with DESeq2. *Genome Biol* 15:550.
- Paxinos G, Franklin KBJ, Franklin KBJ (2001) *The Mouse Brain in Stereotaxic Coordinates* (Academic, San Diego), 2nd Ed.